PAPER

# Tensile behavior of nickel foam/polyurethane co-continuous composites

To cite this article: J X Wang *et al* 2019 *Mater. Res. Express* **6** 095103

Materials Research Express

PAPER

# Tensile behavior of nickel foam/polyurethane co-continuous composites

RECEIVED
15 April 2019

REVISED
9 June 2019

ACCEPTED FOR PUBLICATION
5 July 2019

PUBLISHED
17 July 2019

J X Wang[1,2], D L Duan[1,2], X G Yang[1], M Y Li[1] and S Li[1,2]

[1] Institute of Metal Research, Chinese Academy of Sciences, 72 Wenhua Road, Shenyang 110016, People's Republic of China
[2] School of Materials Science and Engineering, University of Science and Technology of China, 96 JinZhai Road, Hefei 230026, People's Republic of China

**E-mail:** duandl@imr.ac.cn

**Keywords:** Co-continuous composites, tensile properties, synergistic deformation, nickel foam, polyurethane

## Abstract

Six kinds of nickel foam/polyurethane co-continuous composites were successfully prepared by vacuum feeding. The effects of pore size, volume density and metal arris thickness on the tensile properties of nickel foam/polyurethane co-continuous composites were investigated. The relationship between the tensile strength and elongation at break of the composite and the structural parameters of the nickel foam was established, which can be used to estimate the tensile strength and elongation at break of the composite. The nickel foam reinforced composite with moderate metal arris wall thickness had high elongation at break, and the metal phase and the resin phase had good synergistic deformation ability, which can effectively improve the tensile properties of the composite. While increasing the strength, the metal skeleton also had a good toughening effect on the polyurethane.

## 1. Introduction

Co-continuous composites are composed of two components (ceramic and metal generally). The two phase presents respective continuous and network interpenetrating structure in space. In 1992, Clarke [1] officially put forward the concept of co-continuous composites. Co-continuous composites have the advantages of small density, high specific strength, high heat conductivity, high electrical conductivity and good wear resistance due to the unique structure. A lot of research works were carried out on co-continuous composites [2–10] and were mostly about metal/ceramic co-continuous composites such as $Al_2O_3$/Al and SiC foam/Al co-continuous composites. The research on metal/resin co-continuous composites has not been fully exploited.

Polyurethane (PU) elastomer, also known as PU rubber, is a kind of block polymer. A PU macromolecule is composed of soft segments and hard segments. Oligomer polyols's flexible long chains constitute soft segments while diisocyanate and chain extender constitute hard segments. Soft segments and hard segments are arranged alternately. Soft segments have high-elastic state while hard segments constitute a glassy state. PU elastomer has a good ability to elastic deformation, good damping performance and good corrosion resistance. But its application is significantly restricted because of the low strength [11, 12]. PU was strengthened by adding fillers. The strengthen forms are as follow: I particle reinforcement (0 dimension), adding $SiO_2$ and $Al_2O_3$ particles [13, 14]; II fiber reinforcement (1 dimension), adding glass fibers and carbon fibers [15, 16]; III layer reinforcement (2 dimension), adding glass and quartz fiber fabric [17, 18]. These strengthen forms have disadvantages such as reinforcement phase discontinuity and anisotropy. And co-continuous composites can show better performance [19, 20]. In view of the corrosive medium erosion condition, the authors prepared the Ni foam/PU co-continuous composites using the method of vacuum feeding. Ni foam is a common porous metal material whose pores are interconnected and metal arris are arranged continuously in space. Ni foam has high strength and good corrosion resistance [21]. Ni foam/PU co-continuous composites are constructed by interpenetration of the PU and the Ni foam into each other, therefore a co-continuous structure which shows the combined advantages of the PU and the Ni foam is formed.

**Table 1.** Different specifications of the Ni foam.

| Order number | PPI | Pore size μm | Volume density g $cm^{-3}$ |
|---|---|---|---|
| 1 | 100 | 254 | 0.8 |
| 2 | 50 | 508 | 2.3 |
| 3 | 50 | 508 | 1.3 |
| 4 | 50 | 508 | 0.5 |
| 5 | 25 | 1016 | 1.7 |
| 6 | 25 | 1016 | 0.8 |

**Table 2.** Chemical composition of the bicomponent PU glue.

| | |
|---|---|
| Component A | 2, 6—TDI (toluene-diisocyanate) polyester-type prepolymers |
| Component B | Dihydric alcohol chain extender (curing agent) |

Mechanical properties are the basic material nature with great influence on the service performance of the material [22, 23]. The mechanical behavior characteristics of co-continuous composites are particularly noteworthy. Dukhan *et al* [24] prepared aluminum foam–polypropylene interpenetrating phase composites with three kinds of pore sizes through an injection molding process. The stiffness of the composites was found to increase with decreasing pore size. The smaller pore size allowed more cells to exist across the thickness of the specimen, and thus increased the bending stiffness of the composite. Lu *et al* [25] prepared co-continuous $Si_3N_4$/Al composites with different Al content through the squeeze casting. When the volume percentage of Al increased, the Vickers hardness of the composite decreased, the flexural strength decreased and the fracture toughness increased. The rod-like beta-$Si_3N_4$ grains contributed to the fracture toughness of composites by pull-out, crack deflection and crack bridging. Liu *et al* [26] prepared a new SiC/2024Al co-continuous composite with lamellar microstructure by freeze casting. The high mechanical properties of composite are the results of comprehensive effects of few defects, lamellar microstructure and clean and well bonded interfaces between the metal and ceramic phase. Crack deflection and plastic deformation at crack tip in Al phase is the main toughening mechanism in these composites. Sang, Kezheng *et al* [27] prepared interpenetrating $Al_2O_3$/Cu composites. The bending strength of the composites increased with increase of the ceramic fraction, and failure of the composite occurred by ductile fracture of the metal followed by fracture of the ceramic. Liu *et al* [28] studied mechanical behavior of aluminum foam/PU interpenetrating phase composites under monotonic and cyclic compression. The cyclic test results reveal that the recoverable deformation of composites derives from the elastic deformation of Al foam skeleton and the hyper-elastic deformation of PU. It can be noted that the mechanical properties of co-continuous composites are influenced by the mechanical properties of two component materials, and are also influenced by structure factors such as the pore size and volume fraction. The metal/ceramic co-continuous composites widely existed the shortcomings such as poor two-phase interface wettability, weak interfacial bonding, mismatch when the two phase deformed and fractured. In this article, tensile test of Ni foam/PU co-continuous composites were carried out. The factors influencing the composites tensile properties such as pore size, metal arris thickness and volume density were discussed.

## 2. Experimental

### 2.1. Material preparation

Table 1 shows the six kinds of specifications of the Ni foam selected. The different specifications were produced in JiLinZhuoEr new materials co company limited. The PU glue sinwe9603 used was produced in ShenZhenXinWei new materials company limited with chemical components presented in table 2.

The PU glue component A and component B were mixed in proportion, and were injected into the pores of Ni foam using the method of vacuum feeding, curing at room temperature, as shown in figure 1. Prepared foam Ni/PU co-continuous composites were filled completely with few holes. Metal phase and resin phase formed unique interpenetrating network structure. Figure 2 is the macro photos of prepared foam Ni/PU co-continuous composites 50PPI 2.3/PU.

### 2.2. Tensile test

Referring to Chinese standard GB/T228.1-2010, the prepared foam Ni/PU co-continuous composites were machined into the predetermined size with CNC milling machine for tensile tests using German Zwick/Roell

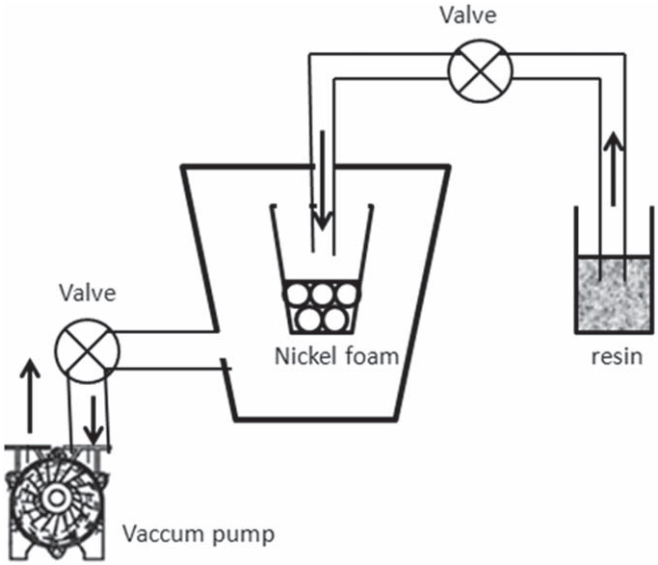


**Figure 1.** Schematic diagram of the vacuum feeding apparatus.

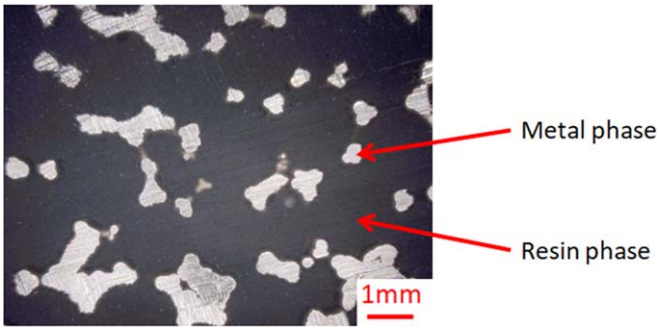


**Figure 2.** Ni Foam/PU co-continuous composite 50PPI 2.3/PU surface morphology.

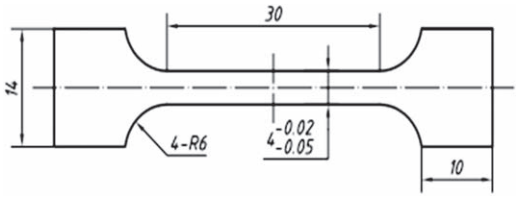


**Figure 3.** Tensile text sample size.

company electron—tensile tester Z050. The sample size is shown in figure 3. The sample thickness is 4 mm. The loading rate was 0.5 mm $min^{-1}$. The Ni foam was processed into a specified size using a wire cut electric discharge machine, as shown in figure 3, 4 mm in thickness. The tensile test conditions were consistent with the tensile test of the Ni foam/PU co-continuous composite. Each tensile test was repeated at least three times to get reliable results. The sample fracture morphologies after tensile test were observed with Japanese keyence company digital microscope VHX—6000 and American FEI company scanning electron microscopy (SEM) Inspect F50.

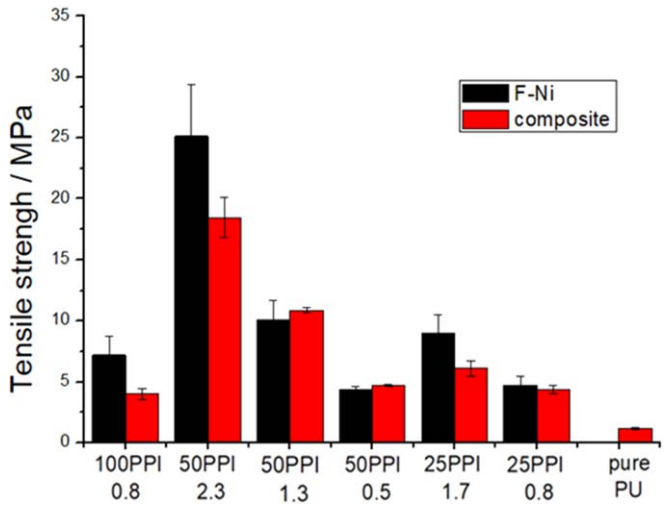


**Figure 4.** The tensile strength of Ni foams (F-Ni), composites and the pure PU (PU).

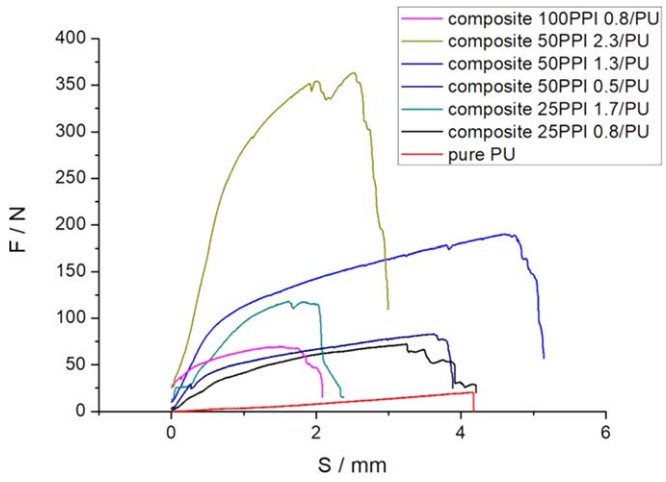


**Figure 5.** Load and displacement curves of composites and pure PU.

## 3. The experimental results and discussion

### 3.1. The tensile strength and fracture morphology

As you can see in figure 4, the tensile strength of all Ni foams and composites is much higher than pure PU. The tensile strength of the composite 50PPI 1.3/PU and 50PPI 0.5/PU is higher than that of the corresponding Ni foam, and the others is reversed. For composites, when the pore sizes are the same, the higher the volume density of Ni foam are, the higher the tensile strength of corresponding composites. When volume density of Ni foam is low, tensile strength difference of different pore size composites is small. When volume density is high, the tensile strength of the 50 PPI composites is significantly higher than 25 PPI composites.

As you can see in figure 5, as the load increases, elongation of pure PU presents the approximate linear growth, breaking at the highest point. For composites, the obvious elastic deformation stage can not be seen in load-displacement curve. In the stage of plastic deformation, the slope of load-displacement curve gradually dwindles until sample breaking.

The tensile curve of the composites is not smooth with a big or small jump, which is related to the inconsistency in the deformation and fracture of the metal phase and resin phase inside the composite, as discussed in detail in section 3.4.

In figure 6, the elongation at break of the composites is much less than that of the corresponding Ni foam. This is because PU can restrict deformation of Ni foam. For these composites, with low volume densities and large pore size, then the larger the elongation at break of composite is. When volume densities are high, the

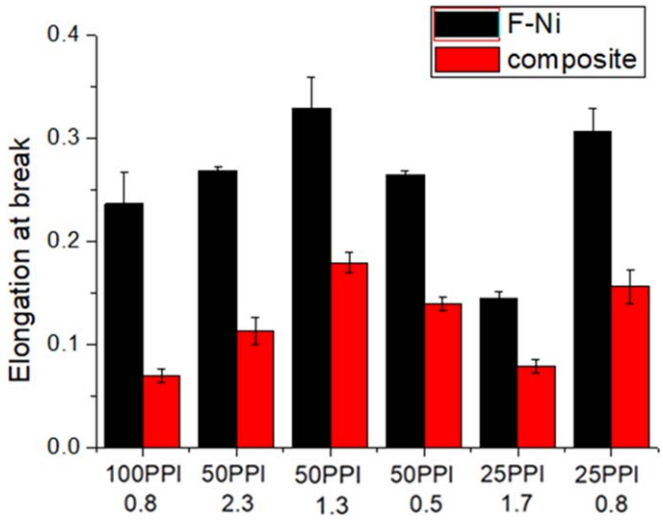


**Figure 6.** The elongation at break of Ni foams and composites.

elongation at break of the 50 PPI composites is significantly higher than 25 PPI composite. In addition, elongation at break of the pure PU obtained was 14%.

Figure 7(a) is pure PU fracture. As shown, the crack was initiated at the edge and corner of the sample, and extended to the diagonal place, making the whole resin fracture. The fracture surface was smooth, and perpendicular to the loading direction, presenting the characteristics of brittle fracture. White bright lines on the fracture showed the direction of crack propagation.

Figure 7(b) is a photograph of the tensile fracture of the composite 25PPI 1.7/PU. It can be seen that the three resin fractures A, B and C on both sides of the fracture correspond to each other, and the gap between the left A, B and C resin fractures was smooth. The smooth resin phase was maintained after the metal phase and the resin phase are debonded. The corresponding metal phase can be seen between the right A, B and C. When the metal arris in the composites was approximately perpendicular to the direction of the force, the metal arris will be separated from the resin phase under the tensile stress. When the metal arris was approximately parallel to the direction of the force, the metal arris will deform locally and fracture under the tensile stress. Three kinds of fracture morphology of composites: resin phase fracture, metal phase fracture and debonding of resin phase and metal phase was obtained. Therefore, the fractures of the composites are scraggly, and the tensile strength increased. Similar morphologies also appear in other composites, as shown in figure S1.

### 3.2. Effect of foamed Ni structure on composites tensile behavior

From 3.1 the tensile behavior of the composites is heavily affected by the Ni foam metal skeleton. To understand the Ni foam structure clear its preparation method is introduced as follows: the organic foam was electrically conductively treated, and the metal layer was electroplated, then the organic foam was removed by burning, and finally Ni foam was heat-treated. Therefore, the Ni foam metal arris had a hollow triangular prism structure, as shown in figure 8. Figure 9 is a schematic diagram of a single metal arris. Table 3 gives the metal arris structure parameters of different Ni foams. a is the thickness of the galvanized coating (metal arris wall thickness), and b is the side length of the triangular prism section.

Gibson and Ashby's studies [29] have shown that at high porosity, the tensile strength of the metal foam was proportional to the 1.5th power of the relative density. For Ni foam/PU co-continuous composites, the authors found:

First, set the variable k,

$$k = \frac{a^{1.7}}{P^2} \tag{1}$$

Where a is the metal arris wall thickness, the unit is $\mu$m; P is the pore size, the unit is $\mu$m. Figure 10 is obtained by curve fitting the data using software origin 8.0.

The fitting curve equation is

$$t = 1704k + 1.4064 \tag{2}$$

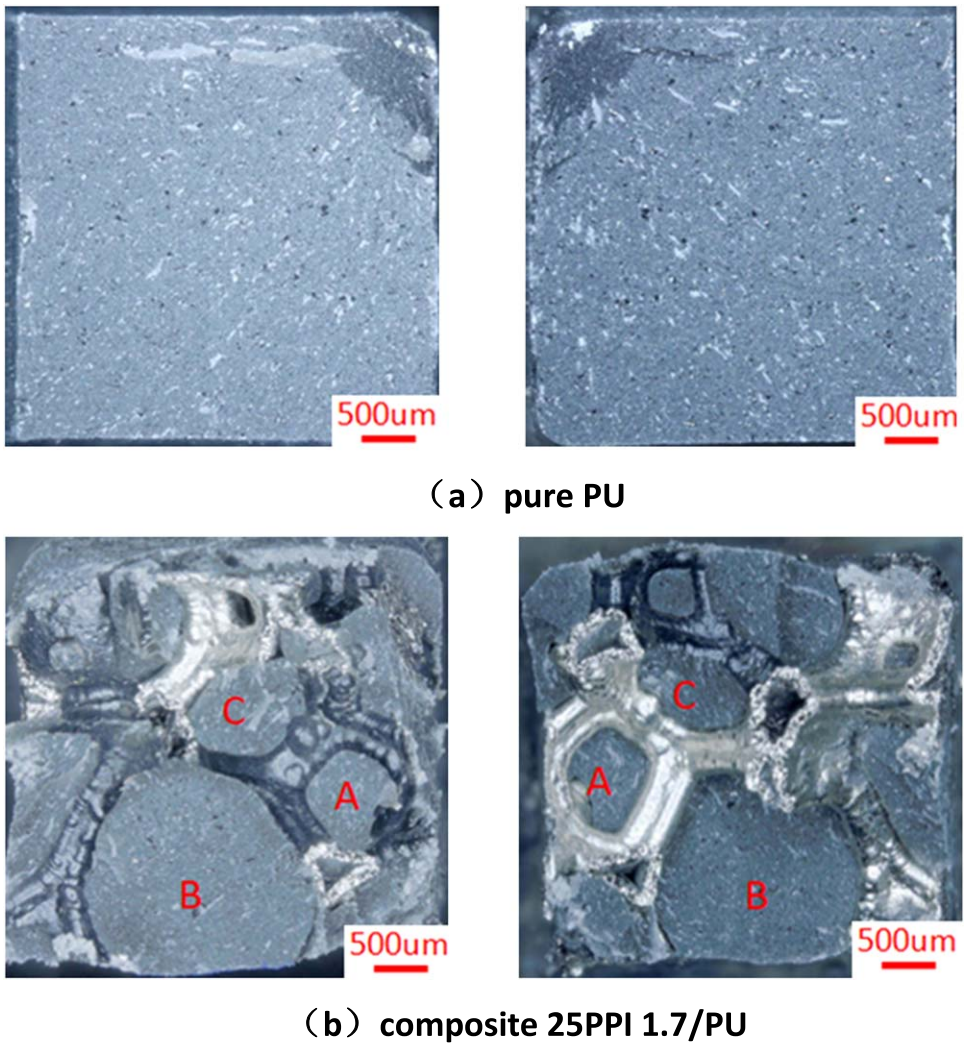


**Figure 7.** The tensile fracture morphology.

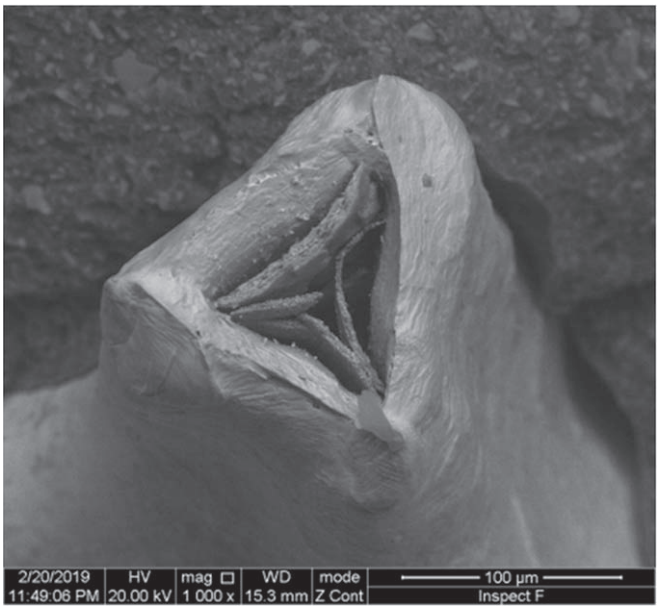


**Figure 8.** The tensile fracture morphology of composite 50PPI 1.3/PU.

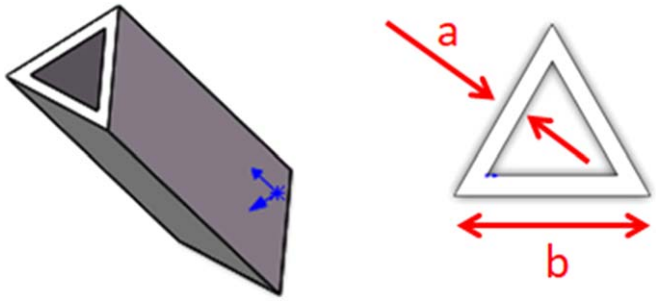


**Figure 9.** Schematic diagram of metal arris and metal arris section.

**Table 3.** Metal arris structure parameters of different Ni foams.

| Ni foam | Thickness a $\mu$m | Length b $\mu$m |
|---|---|---|
| 100PPI 0.8 | 21 | 115 |
| 50PPI 2.3 | 102 | 346 |
| 50PPI 1.3 | 59 | 230 |
| 50PPI 0.5 | 30 | 173 |
| 25PPI 1.7 | 125 | 503 |
| 25PPI 0.8 | 87 | 411 |

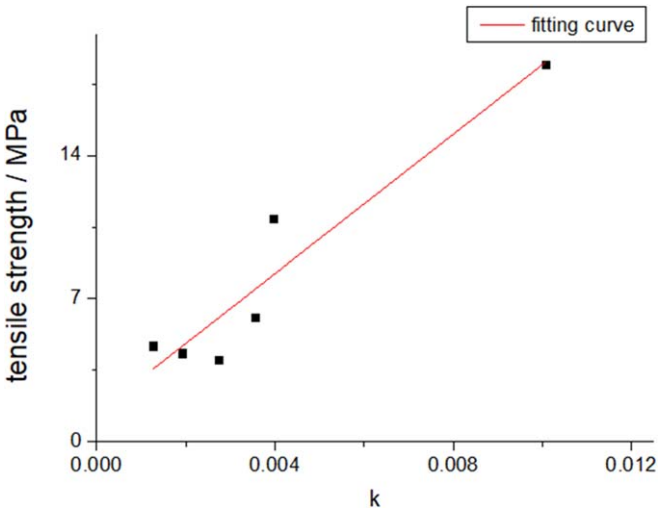


**Figure 10.** Relationship between k and tensile strength.

which is

$$\begin{aligned} t &= 1704\frac{a^{1.7}}{P^2} + 1.4064 \\ R &= 0.952\ 12 \\ F &= 0.003\ 38 \end{aligned} \tag{3}$$

Where t is the tensile strength, the unit is MPa; R is the correlation coefficient, the more tending to 1, the better the fitting effect; F is the confidence probability, the more tending to 0, the better the fitting effect. It can be seen from equation (3) that the thicker the metal arris wall is, the higher the tensile strength of the composite. $P^2$ represents the cross-sectional area of the pore. The smaller the sectional area was, the denser the metal arris distribution. The physical meaning of equation (3) was that in the Ni foam/PU co-continuous composites, the metal arris was thick and densely distributed, and the composites had high tensile strength. It can be seen that the tensile strength of the composites are mainly determined by the structure of the Ni foam.

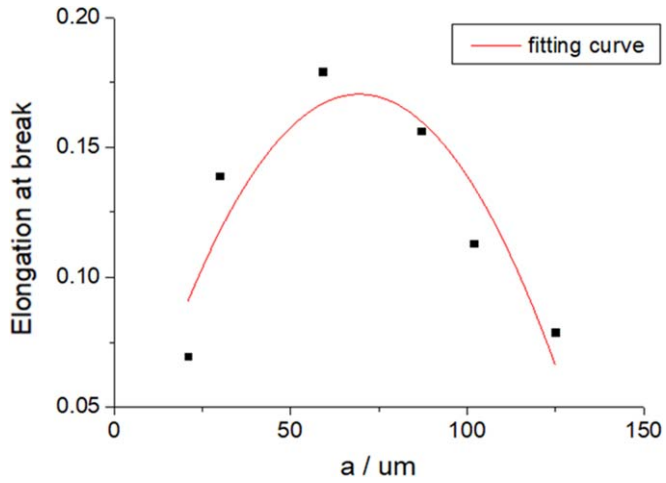


**Figure 11.** Relationship between wall thickness of metal arris a and elongation at break.

**Table 4.** Different specifications of the Ni foam/PU co-continuous composites.

| Composite sample | Composite density (g cm$^{-3}$) | $Ni_{vol\%}$ | $PU_{vol\%}$ |
|---|---|---|---|
| 100PPI 0.8/PU | 2.3 | 8.99 | 91.01 |
| 50PPI 2.3/PU | 3.5 | 25.84 | 74.16 |
| 50PPI 1.3/PU | 2.7 | 14.61 | 85.39 |
| 50PPI 0.5/PU | 2 | 5.62 | 94.38 |
| 25PPI 1.7/PU | 3 | 19.1 | 80.9 |
| 25PPI 0.8/PU | 2.3 | 8.99 | 91.01 |
| Pure PU | 1.6 | — | — |

The fitting curve equation in figure 11 is

$$\begin{aligned}\delta &= -3.383 \times 10^{-5}a^2 + 0.0047a + 0.007\ 13\\ R &= 0.904\ 56\\ F &= 0.077\ 49\end{aligned} \tag{4}$$

Where $\delta$ is the elongation at break; a is the metal arris wall thickness, the unit is $\mu$m; R is the correlation coefficient; F is the confidence probability. It can be seen from equation (4) that if the metal arris wall thickness is too large or too small, the elongation at break will be reduced. Composites with moderate metal arris wall thickness had larger elongation at break.

### 3.3. Synergism of Ni foam and PU

The studies of Zhang *et al* [30] and Nurazzi *et al* [31] have shown that good synergy between the reinforcing phase and the matrix can greatly improve the mechanical properties of the composite. Therefore, in this section the effect of Ni foam structure on synergy was discussed further. According to the compound mixing law [32], this paper proposes synergistic factor Q as follows,

$$t_{composite} = Q \times (t_{Ni} \times Ni_{vol\%} + t_{PU} \times PU_{vol\%}) \tag{5}$$

Equation (5) indicates that the reinforcement phase and the matrix are weighted averaged to estimate the tensile strength of the composite. Where t is the tensile strength, the unit is MPa; vol% is the volume fraction. Q is the synergistic factor of PU and Ni foam. The volume fraction of the resin phase in the composite is calculated according to formula (6).

$$\rho_{composite} = \rho_{Ni\ foam} + \rho_{PU} \times PU_{vol\%} \tag{6}$$

Where $\rho$ is the volume density, $\rho$ is measured by the weighing drainage method. The volume fraction of the metal phase in the composite is the quotient of $\rho_{Ni\ foam}$ and $\rho_{Ni}$. The specific results can be seen in table 4.

$t_{Ni} \times Ni_{vol\%}$ was considered to be the nominal tensile strength value of the Ni foam as shown in figure 4, and the Q value of the different composites are calculated, as shown in figure 12. It can be seen that all Q values are between 0.5 and 1. This may be due to the interlocking of the interpenetrating network structure, which hinders

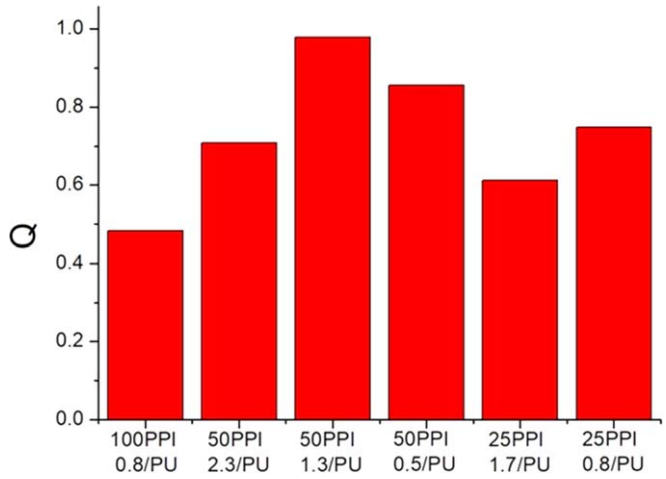


**Figure 12.** The Q values of the different composites.

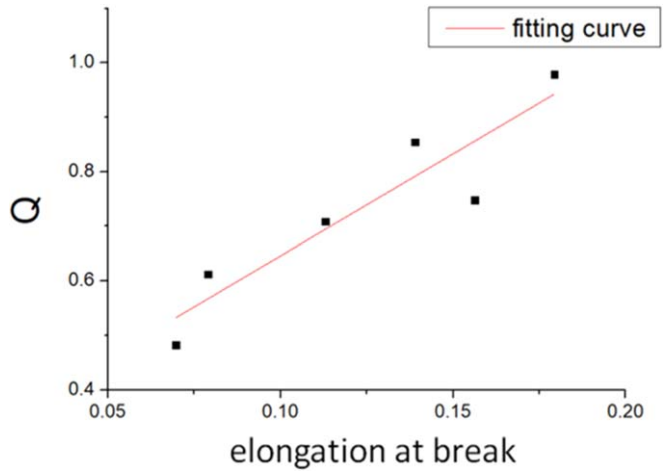


**Figure 13.** Relationship between Q and elongation at break.

the structural deformation of the Ni foam as shown in figure 6 and causes the tensile strength of the metal arris in the composite to decrease.

The fitting curve equation in figure 13 is

$$\begin{aligned} \mathrm{Q} &= 3.7376 \times \delta + 0.272\,13 \\ \mathrm{R} &= 0.926\,02 \\ \mathrm{F} &= 0.008\,01 \end{aligned} \tag{7}$$

Where $\delta$ is the elongation at break; R is the correlation coefficient; F is the confidence probability. As shown in figure 13, the Q value is linearly related to the elongation at break. The elongation at break of the composite is large, indicating that the synergistic deformation ability of the PU and the Ni foam was good. This implies that the PU minimizes the influence on the deformation of the Ni foam. The Ni foam does not reduce the deformation of the PU, whereas increases the deformation amount, such as composite 50PPI 1.3/PU. When the elongation at break increases, the Q value increases, indicating that the good synergistic deformation of the PU and the Ni foam was beneficial to increase the tensile strength of the composite. If the thickness of the metal arris wall was too large or too small, the elongation at break will be reduced and the Q value will be lowered. Therefore, when the metal arris wall thickness was moderate, the synergistic deformation ability of the PU and the Ni foam was good, and the tensile strength of the PU can be effectively improved.

### 3.4. Tensile fracture process and toughening mechanism

Under the tensile stress, the soft segment of the molecular chain undergoes elastic deformation. As the stress increases, the molecular chain begins to slip, the hydrogen bond between the molecular chains breaks, and the molecular chain is oriented in the direction of the force until the molecule chain break [33]. Since the hard

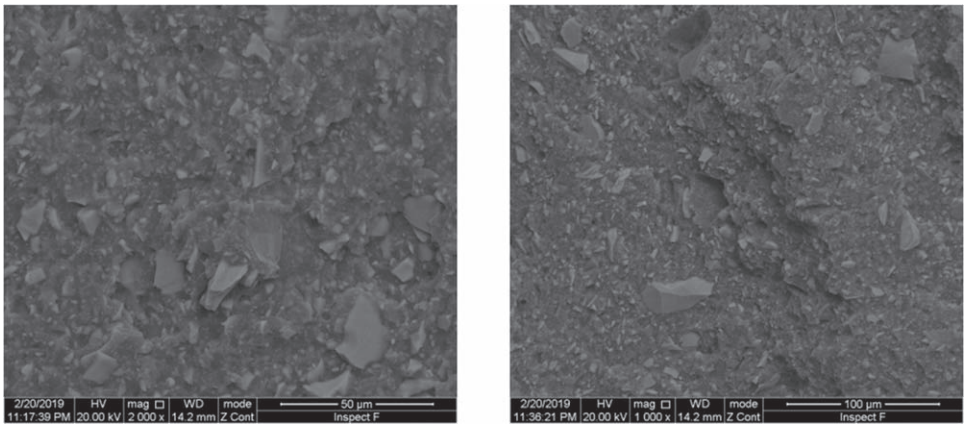


**Figure 14.** The tensile fracture morphology of pure PU.

segment in the molecular chain was in a glassy state, the pure PU exhibited the characteristics of a brittle material once the fracture occured. A large amount of debris was formed on the fracture, as shown in figure 14. Due to some undulations in the fracture, some fragments of specific height and specific angle showed white bright lines under optical microscope observation, as presented in figure 7(a).

The deformation and fracture process of composites under tensile load can be divided into three stages: I. Metal phase and resin phase undergo elastic deformation; II. Resin phase undergoes elastic deformation and metal phase undergoes plastic deformation; III. Resin phase and metal phase debond and fracture, the entire composite fractures. It should be noted that the plastic deformation of the metal phase was composed of two parts. First part was the structural deformation of metal arris such as collapse of the pore structure, bend of some metal arris in the direction of the force. Second part was crystal deformation of the metal phase. In the stages I and II, the resin phase and the metal phase deform synergistically. In the later stage II, as the tensile stress increased, the resin phase and the metal phase no longer deform synergistically, and the two phases deformed respectively and mutually hinder deformation. In the early stage III, some interface debonds and a few weak metal arris and resin phase fracture. Thus, the rigidity of the whole material decreased meaning that the slope of the load-displacement curve gradually decreases. Finally, a few metal arris are simultaneously bearing the load, and fracture when they reach the limit of structural deformation and crystal deformation. After the resin phase breaks, the elastic deformation was returned.

The Ni foam had a similar regular dodecahedral structure [34], and the Ni foam/PU co-continuous composite can be considered to be composed of a number of regular dodecahedral units. Each unit is composed of twelve pentagonal metal arris wrapped with PU, and the interface between the unit and the unit was a resin phase surrounded by pentagonal metal arris. The tensile fracture in figure S1 is multi-celled and dodecahedral unit can be seen individually. But in some areas there will be a large piece of flat resin phase fracture. In the tensile test, the load increased from small to large, and the main crack initiated at the weakest internal defected. When the main crack propagation was subjected to large resistance, the secondary crack began to initiate and propagate. When the main crack passed through a large area, the tensile fracture will have a large area of smooth resin phase. The main crack tends to expand inside the resin phase and at the interface of the two phases. When a metal arris perpendicular to the crack propagation direction was encountered, crack bridging and crack deflection occurred. The secondary crack had a small driving force and a short stroke, and converges inside the respective dodecahedral units, leaving a multi-cell structure after the fracture. When a crack spreads from one unit to another then the propagation direction changes. The breakage of the resin phase occurred at the interface between the unit and the unit, presenting a small piece of resin fracture; or occurs inside the unit, presenting a large piece of resin fracture, as shown in figure 15.

The tensile fracture work was the area obtained by integrating the load-displacement curve of figure 5, which can reflect the toughness of the material to some extent. Figure 16 shows the tensile fracture work of different composites and PU. It can be seen that the tensile fracture work of all composites was much higher than that of pure PU. When the volume density was low, the tensile fracture work of the 100PPI composite was the smallest; when the volume density was high; the tensile fracture work of the 50PPI composite was significantly higher than that of the 25 PPI composite. Tensile strength and elongation at break work together to affect the toughness of the material. When the metal arris wall was thick, the tensile strength was high, but the elongation at break was low. So the thickness of the metal arris was increased, and the Ni foam /PU co-continuous composite were not necessarily toughened. The toughening of PU by foamed Ni includes the following five aspects (1) Toughness

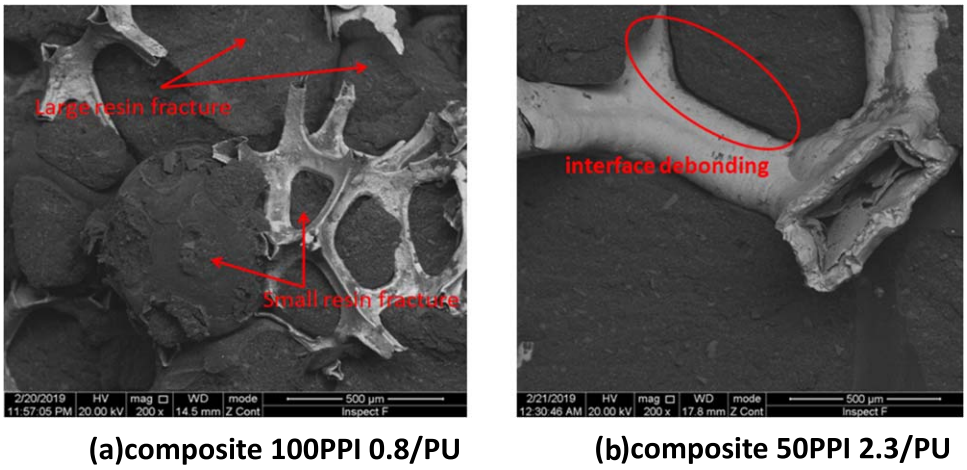


**Figure 15.** The tensile fracture morphology.

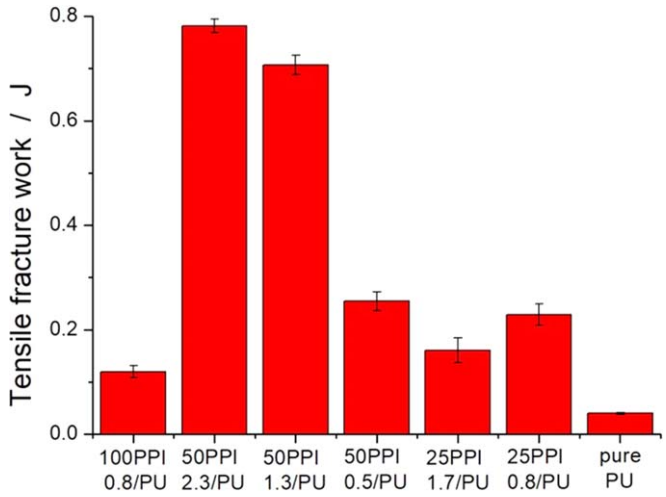


**Figure 16.** Tensile fracture work of composites and pure PU.

fracture of metal arris. Metal arris act as a ductile phase and required to absorb a large amount of energy during fracture (2) Metal arris deformation needed to overcome its own resistance to work (3) Metal arris deformation needed to overcome the binding of the resin phase to work (4) Metal arris deformation needed to overcome the two-phase interface resistance to work (5) Resistance to crack propagation. Some cracks generated at defects such as pores inside the resin, and crack propagation encountered metal arris, causing crack bridging and crack deflection. Some cracks initiated at the interface of the two phases and expanded along the two-phase interface until they converge with other cracks. These crack propagations consume energy. Therefore, the Ni foam can not only increase the strength of the PU but also increase its fracture toughness.

## 4. Conclusion

(1) Six kinds of Ni foam/PU co-continuous composites were successfully prepared by vacuum feeding.

(2) The relationship between the tensile strength and elongation at break of the composite and the structural parameters of the Ni foam was established, which can be used to estimate the tensile strength and elongation at break of the composite.

(3) The Ni foam reinforced composite with moderate metal arris wall thickness had high elongation at break, and the metal phase and the resin phase had a good synergistic deformation ability, which can effectively improve the tensile properties of the composite.

(4) Due to the toughening of the metal skeleton in many aspects, the tensile strength and tensile fracture work of the composites are much higher than pure PU. Compared with other composites and pure PU, composite 50PPI 1.3/PU had high tensile strength, elongation at break and tensile fracture work, whose mechanical property was the best.

## Acknowledgments

Many thanks to the National Natural Science Foundation of China No.51275506, for the support.

## ORCID iDs

J X Wang https://orcid.org/0000-0003-4280-1466

## References

[1] Clarke D R 1992 Interpenetrating phase composites *J. Am. Ceram. Soc.* **75** 739–58
[2] Breslin M C *et al* 1995 Processing, microstructure, and properties of co-continuous alumina-aluminum composites *Materials Science and Engineering:* A **195** 113–9
[3] Lu P *et al* 1999 Interfacial microstructure formed by reactive metal penetration of Al into mullite *J. Mater. Res.* **14** 3530–7
[4] Badini C, Pavese M and Puppo D 2002 Processing of co-continuous ceramic composites by reactive penetration method: influence of composition of ceramic preforms and infiltrating alloys *Int. J. Mater. Prod. Technol.* **17** 182–204
[5] Manfredi D *et al* 2010 Microstructure and mechanical properties of co-continuous metal/ceramic composites obtained from reactive metal penetration of commercial aluminium alloys into cordierite *Composites Part A: Applied Science and Manufacturing* **41** 639–45
[6] Liu J, Wu J and Binner J 2017 Cutting resistance of metal-ceramic interpenetrating composites *Ceram. Int.* **43** 2815–23
[7] Lee J I and Park E S 2017 In-Situ synthesis of co-continuous aluminum-aluminum nitride composites by arc plasma induced accelerated displacement reaction *J. Alloys Compd.* **729** 171–9
[8] Yang X G *et al* 2018 Preparation and erosion-corrosion behavior of polyetheretherketone (PEEK)/Ni foam co-continuous composites *Science and Engineering of Composite Materials* **25** 289–96
[9] Song X *et al* 2018 Co-continuous piezocomposites with triply periodic phase interfaces for enhanced mechanical flexibility and piezoelectricity *ASME 2018 13th Int. Manufacturing Science and Engineering Conf.* (American Society of Mechanical Engineers) V001T01A020-V001T01A020 (https://doi.org/10.1115/MSEC2018-6704)
[10] Lei C *et al* 2019 Fabrication, microstructure and mechanical properties of co-continuous TiCx/Cu-Cu4Ti composites prepared by pressureless-infiltration method *Ceram. Int.* **45** 2932–9
[11] Avar G, Meier-Westhues U, Casselmann H and Achten D 2012 Polyurethanes *Polymer Science: a Comprehensive Reference* (Amsterdam: Elsevier) pp 411–41
[12] Jiang S *et al* 2015 Effect of surface silanization of carbon fiber on mechanical properties of carbon fiber reinforced polyurethane composites *Compos. Sci. Technol.* **110** 87–94
[13] Petrović Z S *et al* 2000 Structure and properties of polyurethane–silica nanocomposites *J. Appl. Polym. Sci.* **76** 133–51
[14] Zhou R *et al* 2005 Mechanical properties and erosion wear resistance of polyurethane matrix composites *Wear* **259** 676–83
[15] Jiang S *et al* 2016 Multiscale graphene oxide–carbon fiber reinforcements for advanced polyurethane composites *Composites Part A: Applied Science and Manufacturing* **87** 1–9
[16] Ohki T *et al* 2004 Mechanical and shape memory behavior of composites with shape memory polymer *Composites Part A: Applied Science and Manufacturing* **35** 1065–73
[17] Lv G *et al* 2018 The remarkably enhanced particle erosion resistance and toughness properties of glass fiber/epoxy composites via thermoplastic polyurethane nonwoven fabric *Polym. Test* **69** 470–7
[18] Lu H R and Wang C A 2013 Fabrication and characterization of ceramic coatings with alumina–silica sol-incorporated α-alumina powder coated on woven quartz fiber fabrics *Ceram. Int.* **39** 6041–50
[19] Ren Z H *et al* 2015 Mechanical properties and slurry erosion resistance of SiC ceramic foam/epoxy co-continuous phase composite *Compos. Sci. Technol.* **107** 129–36
[20] Li S *et al* 2014 Thermophysical properties of SiC/Al composites with three dimensional interpenetrating network structure *Ceram. Int.* **40** 7539–44
[21] Hatamie A *et al* 2019 Electrocatalytic oxidation of ethanol on flexible three-dimensional interconnected Ni/gold composite foams in Alkaline media *Electroanalysis* **31** 504–11
[22] Chen S *et al* 2015 Mechanical properties of 3D-structure composites based on warp-knitted spacer fabrics *Autex Research Journal* **15** 127–37
[23] Song J, Hu W and Gottstein G 2011 Long term stability and mechanical properties of $Al_2O_3$–NiAl composites reinforced with partially fragmented long fibers *Materials Science and Engineering:* A **528** 7790–800
[24] Dukhan N, Rayess N and Hadley J 2010 Characterization of aluminum foam–polypropylene interpenetrating phase composites: flexural test results *Mech. Mater.* **42** 134–41
[25] Lu Y *et al* 2010 The mechanical properties of co-continuous $Si_3N_4$/Al composites manufactured by squeeze casting *Materials Science and Engineering:* A **527** 6289–99
[26] Liu Q *et al* 2014 Fabrication of a new SiC/2024Al co-continuous composite with lamellar microstructure and high mechanical properties *J. Alloys Compd.* **585** 146–53
[27] Sang K *et al* 2016 Preparation of interpenetrating alumina–copper composites *Ceram. Int.* **42** 6129–35
[28] Liu S, Li A and Xuan P 2019 Mechanical behavior of aluminum foam/polyurethane interpenetrating phase composites under monotonic and cyclic compression *Composites Part A: Applied Science and Manufacturing* **116** 87–97
[29] Gibson L J and Ashby M F 1997 *Cellular Solids: Structure and Properties* 2nd edn (Cambridge: Cambridge University Press) pp 217–21

[30] Zhang J *et al* 2018 The influence of CF and TLCP co-reinforced on the mechanical properties of PA6-based composites *Mater. Res. Express* **5** 055303
[31] Nurazzi N M *et al* 2018 Development of sugar palm yarn/glass fibre reinforced unsaturated polyester hybrid composites *Mater. Res. Express* **5** 045308
[32] Bunsell A R and Harris B 1974 *Composites* **5** **157**
[33] Mingshi S and Yiding S 1989 The ultimate dynamic model theory of the ultimate fracture of thermoplastic polyurethane elastomers *Journal of Beijing Institute of Chemical Technology* **16** 26–33
[34] Duan D L, Zhang R L, Ding X J and Li S 2006 Calculation of specific surface area of foam metals using a dodecahedron model *Material Science and Technology* **22** 1364–7